ELSEVIER

Energy and Buildings 24 (1996) 125–132

ENERGY AND BUILDINGS

Prediction of air temperature distribution in buildings with a zonal model

Christian Inard [a], Hassan Bouia [a], Pascal Dalicieux [b]

[a] *Thermal Engineering Center, National Institute of Applied Sciences, Lyon, France*

[b] *Electricity of France, R&D Division, Building Physics, Moret/Loing, France*

Received 12 April 1995; accepted 20 November 1995

Abstract

This study presents a zonal model used for predicting the air temperature distribution inside a room. This model is original in the calculation of mass air flows between two zones. To do so, we distinguish zones where the momentum is small and for which we calculate the flow rates with the aid of a pressure field, and the driving zones described using appropriate specific flow laws. A comparison between experimental results and those obtained with the model proves that they are fully consistent with each other. This allows us to consider the integration of this type of model into a general building thermal code.

Keywords: Zonal models; Air temperature distribution

1. Introduction

During the last two decades, considerable effort has been made, when modelling the thermoconvective field of a room, to overstep the notion of isothermal air volume which, though a proper sizing tool, does not allow the problems of comparison between the heating and ventilation systems, especially with regard to thermal comfort, energy consumption and indoor air quality. Though an approach to the problem through the CFD codes proves highly serviceable [1], the simplified model we present provides an alternative and inexpensive solution for engineers who could not use the CFD method for their problem.

For this reason, the zonal model principle, which consists in breaking up the indoor air volume into macro-volumes to reach the desired objectives, has been much in use with varying degrees of success. Mass and thermal balances are written for each zone so as to calculate the indoor temperature field. The main problem posed with this type of modelling is the evaluation of mass transfers between the zones considered.

A first approach [2,3] consists in fixing the air flow direction and settling the problem posed by specific flow laws such as plumes and jets. This method yielded consistent results [4,5] but also has a limited field of application owing to its basic hypothesis, namely a fixed air flow pattern.

In other respects, another method [6,7] consists in calculating an indoor pressure field using a 'degraded' equation for the momentum allowing a mass air flow between two zones to be connected to the corresponding pressure differential. Though this method has a more general field of application, its limits become instantly evident when predicting driving flows (plumes, jets, etc.) owing to the poor representation of the momentum for such flows.

A zonal model derived from the approaches we have briefly described is presented in this paper. The model is based upon a representation of the so-called current or low velocity zones by a pressure field while the driving flows are described by their behaviour laws. We thus obtain an increased generality of the model.

2. Description of the model

2.1. General structure of the model

The domain under consideration is broken up into n isothermal zones according to a parallelepipedic geometry. All these zones are inter-connected by mass air flows and the mass and thermal balances are given for each of them.

For the mass balance, we write:

$$\sum_{j=1}^{n} m_{ij} + ms_i = \sum_{j=1}^{n} m_{ji} + me_i \qquad (1)$$

The thermal balance under steady state conditions, is expressed by:

$$\sum_{j-1}^{n} Cpm_{ij}(T_i - T_j) + Cpms_i(T_i - Ts_i) + \Phi_{\text{conv}\,i} = P_{\text{conv}\,i} \qquad (2)$$

SSDI 0378-7788(95)00969-8

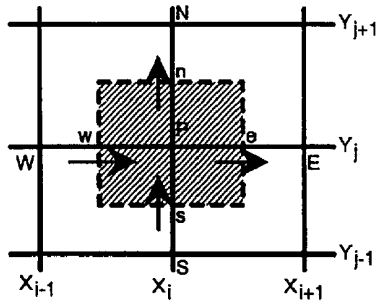

Fig. 1. Example of control volume.

Consequently, if we express the convective heat fluxes exchanged along the walls as a function of air temperatures, we have n independent equations for the thermal balance associated to $n-1$ equations for the mass balance. Generally speaking, we, in fact, have $n+n(n-1)$ that are unknown. The difference between the number of available independent equations and the number of unknown quantities is due to the fact that we do not use the equations of momentum conservation. To settle the problem and to obtain a rapid approximate method, we distinguish two types of zones:

(i) the current zones,

(ii) the specific flow zones.

We thus choose a different procedure for each type of zone to calculate the air mass flows exchanged between two zones.

2.2. Calculation of inter-zone flows

2.2.1. Case of current zones

If we use the finite volume method in association with a staggered grid such as described in Fig. 1, it is shown [8] that rendering discrete equations of momentum conservation according to the directions x, y and z are written:

$$a_e u_e = \Sigma a_{nb} u_{nb} + A_e(P_P - P_E) \tag{3}$$

$$a'_n v_n = \Sigma a'_{nb} v_{nb} + A_n(P_P - P_N) \tag{4}$$

$$a''_t w_t = \Sigma a''_{nb} w_{nb} + A_t(P_P - P_T) - (\rho g \Delta V)_t \tag{5}$$

In order to solve these equations by using, for instance, the SIMPLER algorithm [8], a fine grid discretization of the domain studied is required. We in fact propose using a simplified method taking account of an important characteristic of current zones, namely the uniformity and the low amplitude of the velocities and, consequently, of the momentum. One can therefore rightfully assume that the velocities are mainly governed by variations in the driving pressure. We have therefore developed the simplified method detailed below on the basis of these remarks.

Eqs. (3)–(5) can be written as follows:

$$\left(\frac{1}{2}\rho_e u_e\right) u_e = \epsilon_u C d_u^2 (P_P - P_E) \tag{6}$$

$$\left(\frac{1}{2}\rho_n v_n\right) v_n = \epsilon_v C d_v^2 (P_P - P_N) \tag{7}$$

$$\left(\frac{1}{2}\rho_t w_t\right) w_t = \epsilon_w C d_w^2 ((P_P - P_T) - (\rho g h)_t) \tag{8}$$

with:

$$C d_u^2 = \frac{\left|\frac{1}{2}\rho_e u_e A_e\right|}{\left|a_e - \Sigma a_{nb}\frac{u_{nb}}{u_e}\right|} \tag{9}$$

$$C d_v^2 = \frac{\left|\frac{1}{2}\rho_n v_n A_n\right|}{\left|a'_n - \Sigma a'_{nb}\frac{v_{nb}}{v_n}\right|} \tag{10}$$

$$C d_w^2 = \frac{\left|\frac{1}{2}\rho_t w_t A_t\right|}{\left|a''_t - \Sigma a''_{nb}\frac{w_{nb}}{w_t}\right|} \tag{11}$$

ϵ_u, ϵ_v and ϵ_w, of which absolute value is 1, make the signs of the two members of each of Eqs. (6)–(8) equal. Coefficients Cd_u, Cd_v and Cd_w are analogous to discharge coefficients. This formulation is such that the driving pressure deviation, e.g. $P_P - P_E$ between two adjacent meshes generates a discharging velocity flow u_e which crosses the border between those two meshes with a discharge coefficient Cd_u. Eq. (6) allows the mass flow rate associated to velocity u_e through the interface between the two zones centred in P and E (direction x) to be explained:

$$m_{P\to E} = \epsilon_u \rho_e C d_u A_e \left(\frac{2|P_P - P_E|}{\rho_e}\right)^{1/d} \tag{12}$$

We also obtain a similar relation which expresses the flow exchange between two adjacent zones in the direction y:

$$m_{P\to N} = \epsilon_v \rho_n C d_v A_n \left(\frac{2|P_P - P_N|}{\rho_n}\right)^{1/2} \tag{13}$$

As regards direction z, the density must be taken into account:

$$m_{P\to T} = \epsilon_w \rho_t C d_w A_t \left(\frac{2|(P_P - P_T) - (\rho g h)_t|}{\rho_t}\right)^{1/2} \tag{14}$$

with:

$$(\rho g h)_t = \frac{1}{2}((\rho g h)_P + (\rho g h)_T) \tag{15}$$

As a general rule, we express the mass flow rate which crosses a vertical border between two current zones i and j by the following expression:

$$m_{ij} = \epsilon_{ij}\sqrt{2\rho_j} C d A_{ij} |P_j - P_i|^{1/2} \tag{16}$$

In the case of a horizontal border between two current zones, we write:

$$m_{ij} = \epsilon_{ij}\sqrt{2\rho_j} C d A_{ij} \left|(P_j - P_i) - \frac{1}{2}(\rho_i g h_i + \rho_j g h_j)\right|^{1/2} \tag{17}$$

Eqs. (16) and (17) are used to compute the mass flow rate through the vertical and horizontal borders of the current zones.

The discharge coefficients *Cd* are empirical coefficients including viscous effects and local contraction of the streamlines when the flow crosses an opening. These coefficients have to be determined experimentally by the ratio between the actual air mass flow and the theoretical flow. When there are no solid borders and velocity flows are low, as in our study, it is very difficult to obtain accurate experimental values of the discharge coefficients. Nevertheless, in order to give a proper value to these coefficients and considering that velocities within current zones are very slow (the high velocity flows are described by specific laws), the experimental data obtained for air movement through doorways with natural convection flows were used [9]. In this way, the discharge coefficient values were set to 0.8. Though this value gives consistent results compared to the experimental data, it is clear that more work is needed in order to obtain an accurate discharge coefficient value.

As specified earlier, this approximate formulation of inter-zone mass flow rates is justified only for low-velocity flows but is not convenient for driving flows. The inter-zone mass flow rate in the latter case is calculated by using laws that govern specific flows.

2.2.2. Case of zones with specific flows

For the time being, we have integrated three types of specific flows into the model, namely:

(i) wall anisothermal horizontal jet,

(ii) wall thermal plume derived from a local heat source,

(iii) thermal boundary layer.

Provision has been made for integrating flow models such as free thermal plume and wall anisothermal vertical jet.

The laws applied for each type of flow are as follows:

(i) *Wall anisothermal horizontal jet*– penetration length [10]:

$$Xs = a_1\left(\frac{1}{Ar_o}\right)^{b_1} \tag{18}$$

– mass flow rate [11]:

$$\frac{m(x)}{m_o} = K_1\left(\frac{x}{b_o}\right)^{\alpha} \tag{19}$$

As Eq. (19) includes the discharge air of the jet nozzle, it should be adequate for properly evaluating ambient air entrainment in the jet even for high momentum flows.

(ii) *Wall thermal plume derived from a local heat source*– mass flow rate [12]:

$$m(z) = K_2 Q(z)^{1/3}(z - z_o)^{\beta} \tag{20}$$

(iii) *Thermal boundary layer*– mass flow rate [13]:

$$m(z) = K_3 \Delta T^{1/3} z \tag{21}$$

Table 1 gives values for coefficients used in Eqs. (18)–(21).

Table 1
Values of specific flow coefficients

Plane wall jet	$a_1 = 0.74 b_o$	$b_1 = 2/3$	$K_1 = 0.25$	$\alpha = 0.5$
Plane thermal plume	$K_2 = 0.009$	$\beta = 1$		
Thermal boundary layer	$K_3 = 0.004$			

On the basis of the above-mentioned laws, we can evaluate the ambient air induction rate within the specific flow considered and calculate the mass flow rate of air crossing a border between the specific flow and a current zone.

Writing the mass and thermal balances for each zone is a non-linear system we solve using Broyden's method [14]. Solving this system allows us to know the pressure field (for current zones) and the temperature field (for each zone).

To better understand the consistency of the model results, it was necessary to compare them with the experimental results. Experiments were made in two real-size test cells, and the numerical and experimental results compared in two stages. The first stage consisted in checking the model consistency with basic cases, namely the cell which was thermally driven (natural convection) and that heated by a linear heat source (mixed convection). The model consistency was then checked with cases closer to the reality, i.e. a cell ventilated and heated by real heat emitters.

3. Comparison of the model with the experiment

3.1. Basic cases

Experiments were made in CETHIL's MINIBAT test cell of which a cross section is shown in Fig. 2.

This test cell consists of a 24 m^3 (3.1 × 3.1 × 2.5 m) single volume of which the temperature is kept constant on five faces owing to another volume used as a thermal guard. The sixth face (facing south) is in contact with a climatic caisson which allows us to obtain air temperatures ranging from −10 to +40 °C with a very good stability (±0.2 °C). An insolation simulator made up of twelve 1100 W CSI lamps allows reproduction of the effects of a direct insolation within the cell, and electric films enable the ceiling heating simulation. The cell is equipped with 200 temperature sensors distributed within the volume and surface of the walls that are more especially used to obtain an experimental isotherm field in the cell mid-plane.

A detailed description of the MINIBAT test cell is given in Ref. [15].

As specified earlier, tests were carried out in this cell for two types of flows: natural convection and mixed convection.

3.1.1. Case of natural convection

Four basic cases were dealt with:

Case no. 1: one cold active vertical face;

Case no. 2: one cold active vertical face, the face opposite being heated;

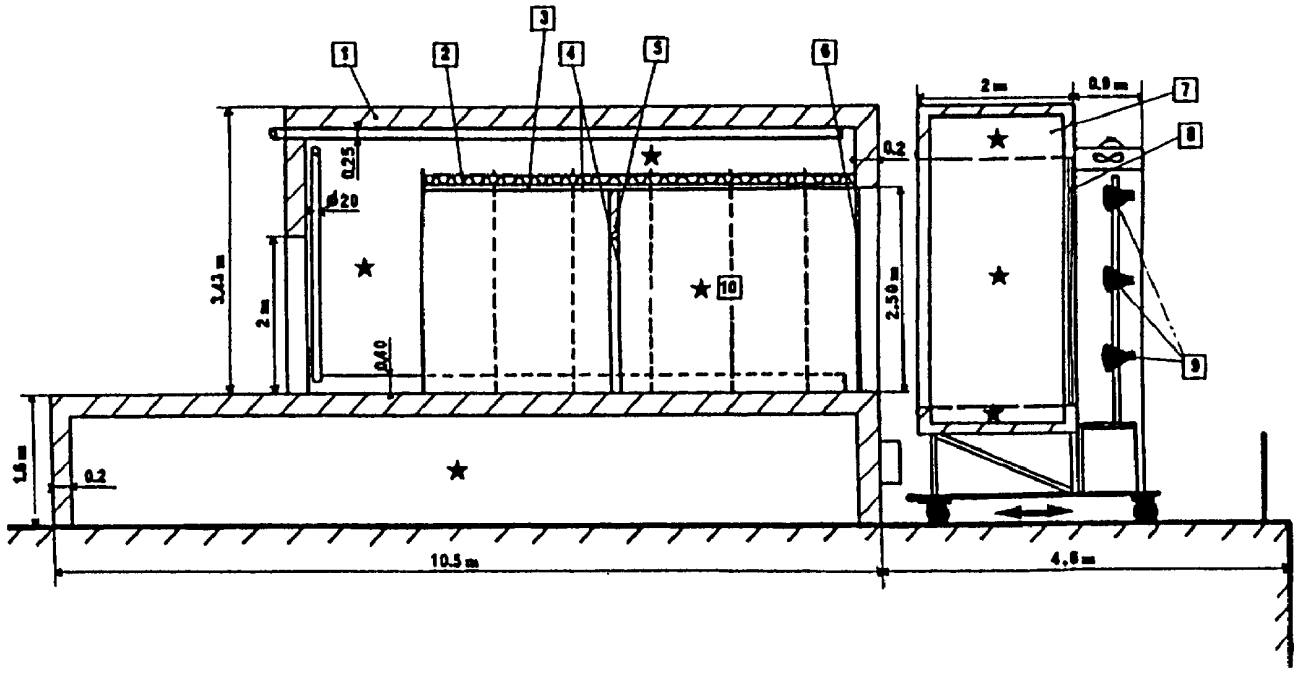

Fig. 2. MINIBAT cell cross section. 1: External casing (cellular concrete, 20 cm thick); 2: glasswool (5 cm thick); 3: plywood (2.5 cm thick); 4: plaster (1 cm thick); 5: fiberboard (5 cm thick); 6: glazing (1 cm thick); 7: climatic caisson; 8: double-glazing (10–8–10 mm); 9: insulation simulator; 10: test cell; *: position of ambient control temperature sensors.

Table 2
Values of average inside temperatures (°C) measured for case nos. 1–4

	South	North	East	West	Ceiling	Floor
Case no. 1	6.0	13.9	14.1	14.1	13.5	11.8
Case no. 2	16.9	33.0	26.9	27.3	28.5	25.9
Case no. 3	15.3	29.1	26.1	26.2	26.0	27.6
Case no. 4	11.2	23.8	23.5	23.7	42.1	21.1

Case no. 3: one cold active vertical face, the floor being heated;

Case no. 4: one cold active vertical face, the ceiling being heated.

Table 2 gives the values of average inside surface temperatures measured for each case.

Owing to the fact that the limit conditions are symmetrical (the surface temperatures of east and west walls are persistently very close), the experiments were modelled with the aid of a 2D meshing with six meshes in the lengthwise direction and ten meshes over the height of the cell. Considering the computational grid, we conducted a dependent study on cell number. The results of this study showed that the computed values are not very sensitive to the cell number in the lengthwise direction and the widthwise direction of the cell owing to low air temperature gradients along these coordinates. On the other hand, we noticed a dependence of the results on the cell number over the height. So, the grid was carried out in order to properly represent both specific flows as thermal boundary layers and experimental vertical air temperature profiles.

First, as an example, we present the computed air mass flows for case no. 2 (see Fig. 3). We observe a downward thermal boundary layer along the cold (south) wall and an upward flow along the hot (north) wall. Then, these flows create an upward movement in the lower part of the cell and

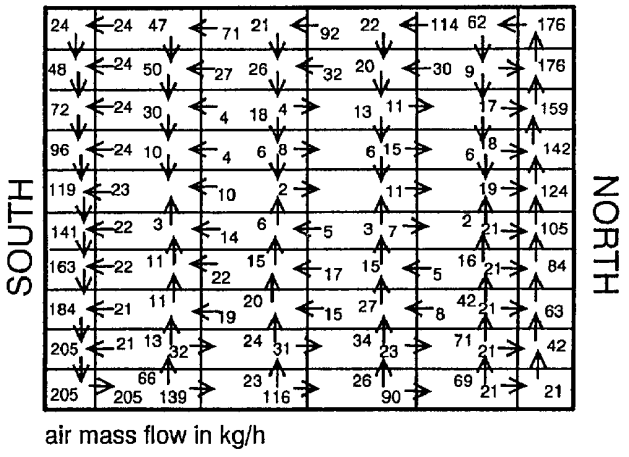

Fig. 3. Calculated air mass flows (case no. 2).

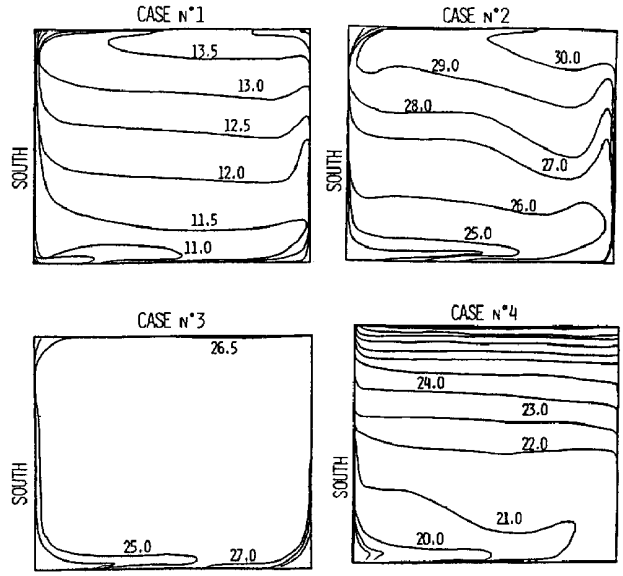

Fig. 4. Isotherms measured in the cell mid-plane (case nos. 1–4).

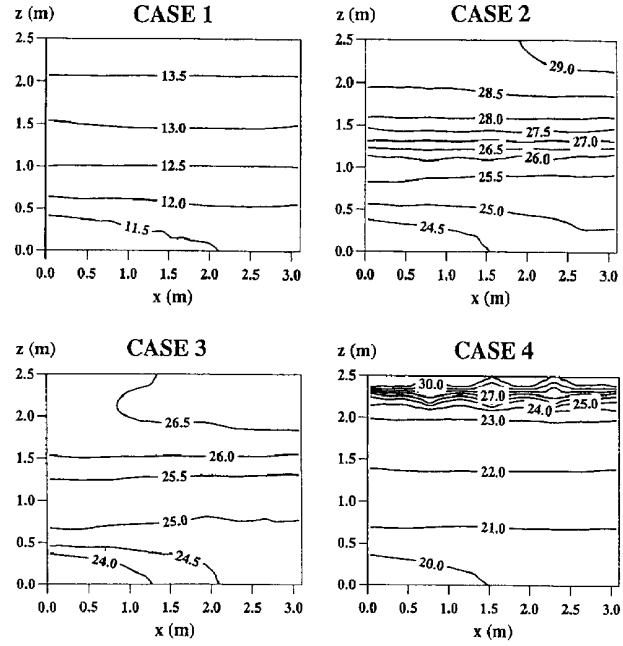

Fig. 5. Calculated isotherms (case nos. 1–4).

a downward flow in the higher part. Lastly, the boundary layers are alimented from the core of the cavity by a slow recirculation satisfying mass continuity.

Isotherms measured in the cell mid-plane and those calculated by the model are noted in Fig. 4 and Fig. 5.

In these figures, we can see that the calculated values of the temperatures are always very close to those measured. It is also interesting to note that the model gives a true representation of the thermoconvective field inside the cell whatever the thermal loads. We thus see for case nos. 1 and 2, a steady stratification of the inside volume which is close to the 'window problem' especially in case no. 2. Case no. 3 shows by experiment an almost perfect isothermy of the inside air volume while the calculation gives a slightly higher gradient. Lastly, in case no. 4, we can see both experimentally and numerically a very high thermal gradient at the top which tends to stop the air flow in the cell zone.

3.1.2. *Case of mixed convection*

With a view to minimising the influence of the heat emitter characteristics, we chose to use for the present study a system which best reproduces a linear heat source with mainly convective emission.

Fig. 6 shows a cross section of the device used.

We thus built three 1 m long heating elements which can be supplied separately and are located along the south wall. Each element is made up of a cylindrical electric heating bar. Of interest also was to see the influence of the heat source concentration over the inside thermoconvective field. For this reason we dealt with two cases:

(i) case no. 5: three electric resistances in service (cold wall fully compensated),

(ii) case no. 6: only the middle electric resistance in service (cold wall partly compensated).

Owing to the configurations dealt with, case no. 5 was simulated with a 2D (6×1×10 zones) meshing and case no. 6 with a 3D (6×3×5 zones) meshing.

As an example, Fig. 7 shows the computed air mass flows for case no. 5. We can notice that the main driving flow is the plume of the linear heat source. When the thermal plume impinges on the ceiling, it spreads on this surface and creates a slow downward flow in the core of the cell which feeds the thermal plume.

In Fig. 8 and Fig. 9, we have noted the isotherms measured in the mid-plane and those computed by the model.

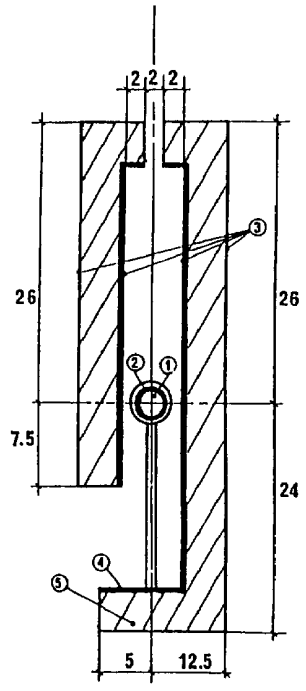

Fig. 6. Heat source cross section. 1: Electrical resistance; 2: alumina insulating ring; 3: aluminized coating; 4: aluminium support; 5: insulator (4 cm thick). Dimensions in cm.

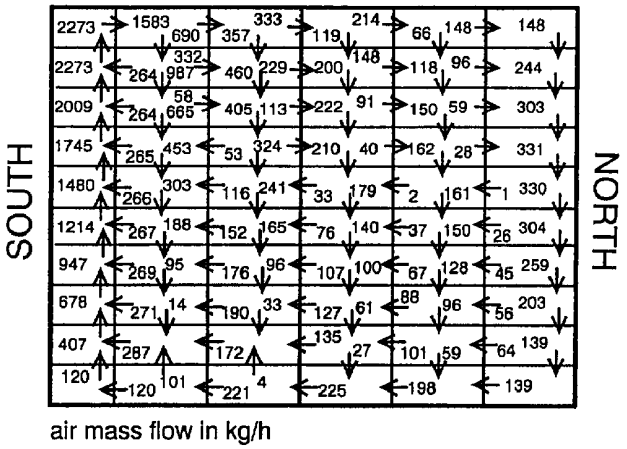

Fig. 7. Calculated air mass flows (case no. 5).

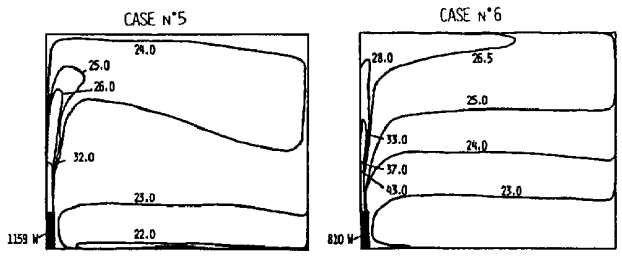

Fig. 8. Isotherms measured in the cell mid-plane (case nos. 5 and 6).

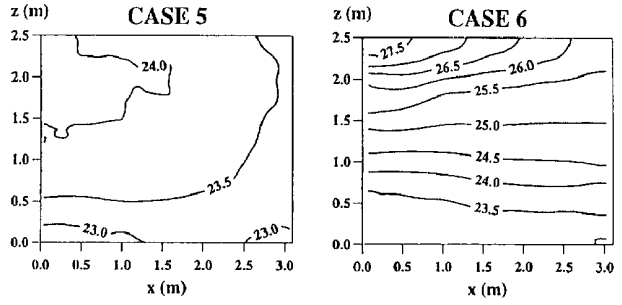

Fig. 9. Calculated isotherms (case nos. 5 and 6).

Table 3
Total and convective heat powers of the emitters

	Frontage temperature			
	12 °C		15 °C	
	P_{tot} (W)	P_{conv} (W)	P_{tot} (W)	P_{conv} (W)
COF	644	592	501	458
PAN	528	272	435	221
HFL	628	269	468	193

There again, we see that the model properly reproduces the physical reality of the phenomena. When the heat source, in fact, fully compensates the cold wall (case no. 5) we obtain an almost isothermal inside air volume both experimentally and numerically. On the contrary, when only the middle resistance is in service (case no. 6) the inside air volume is regularly stratified with horizontal isotherms practically in the whole central volume. This fact is properly reproduced by the model with calculated and measured temperatures which are very consistent.

The comparison of the experimental and numerical results given above is satisfactory for the cases handled. However, as the model we developed is to be integrated into a more general calculation code for predicting the building's thermal behaviour, this comparison should be extended to more realistic cases, namely to a room ventilated and heated with real emitters.

3.2. *Room ventilated and heated with real emitters*

The experiments performed were carried out within the framework of the Groupe de Recherche sur les Emetteurs de Chaleur (GREC) (Heat Emitter Research Group) established by the Agence de l'Environnement et de la Maîtrise de l'Energie (ADEME) (Environment and Energy Management Agency), from Jan. 1990 to Jan. 1995.

The tests we present in this document were performed in the EREDIS test cell of the Building Scientific and Technical Centre (CSTB). All the vertical walls, except for the frontage, and the ceiling are strongly insulated so that the fluxes conducted through them are very low. The floor is fitted with a water circulation system to simulate a floor water heating system. Lastly, the frontage consists of water panels which allow an inner surface temperature to be imposed so as to be able to reproduce different outside conditions. The frontage includes a 1 m high breast-wall made up of a 2 cm layer of insulating material.

A detailed description of the EREDIS test cell is given in Ref. [16].

The cell is ventilated by the fresh air supplied at the top of the frontage and in the cell principal plane. Air is exhausted at the bottom of the wall across the frontage. The air change rate is fixed at 0.5 ach given a fresh air temperature of 4 °C. The frontage temperature is fixed at 12 and 15 °C, respectively.

For the purpose of applying a convective load upon the inside air volume non-continually three types of emitters were chosen, namely:

(i) an electric convector with front air delivery (COF),

(ii) a water heater of the single panel type (PAN),

(iii) a water heating floor (HFL).

Table 3 gives the values of the total and convective powers injected into the room for the two frontage temperatures and the three types of emitters.

According to Table 3, it seems that, given a total emitted power of the same order of magnitude, the convective fraction of the electric convector is about twice that of the other two emitters. In addition, the single panel and the heating floor have convective powers fairly equivalent though the mode of emission (local and distributed) differs.

In this case, we compared the vertical temperature profiles measured and calculated in the middle of the cell (see

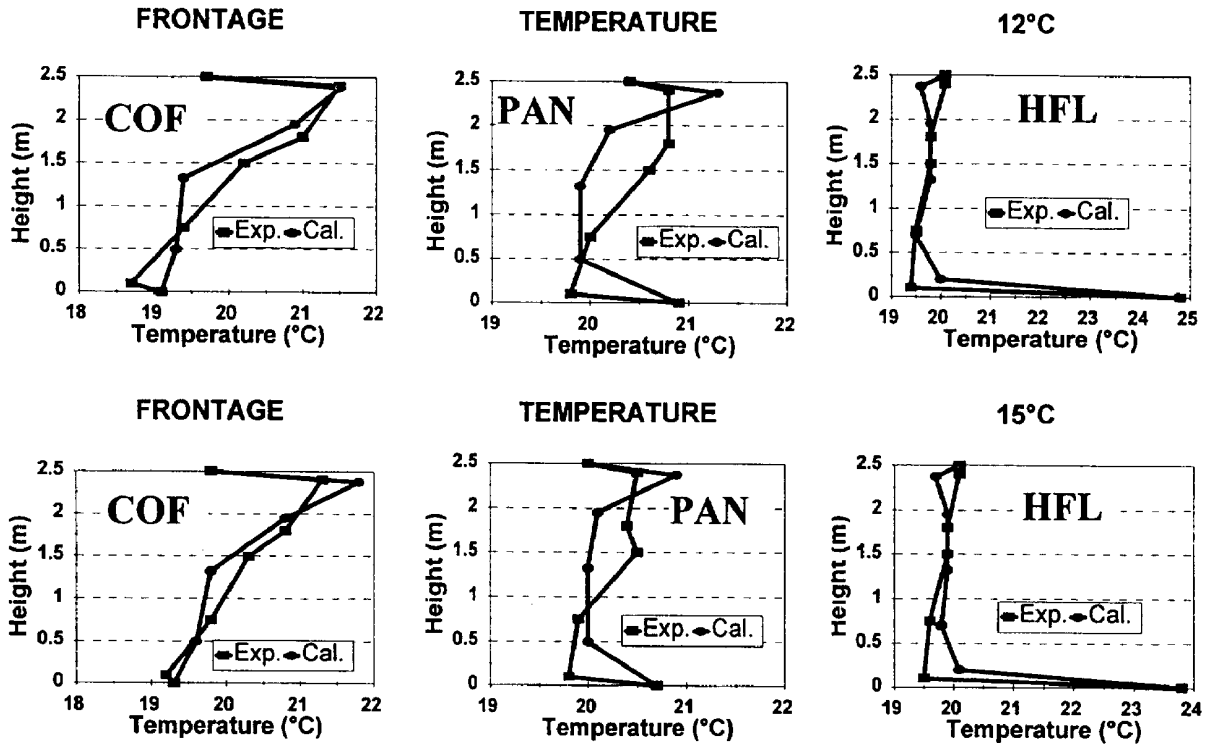

Fig. 10. Vertical air temperature profiles measured and calculated.

Fig. 10). It can be seen that the electric convector establishes a thermal gradient higher than the other emitters which is induced by a higher convective power. Nevertheless, the air temperature differences observed are lower than those recommended by the ISO standard on thermal comfort [17]. Additionally, owing to its low convective power and to its mode of heat emission, the heating floor generates an inside thermoconvective field which is practically isothermal.

It is interesting to point out that the model reproduces these tendencies accurately. The maximum deviation thus seen between the measured and the calculated values is about 0.6 °C, which proves that the numerical and the experimental results are consistent.

4. Conclusions

In this study, we have presented a zonal model with a wide range of applications owing to the calculation of a pressure field for the zones where the momentum is small and to the use of the behaviour laws for the driving flows.

A comparison of the numerical results and the experiment for the basic cases as well as for configurations close to those of dwelling units has proven that the model gives a satisfactory reproduction of the thermoconvective field in a heated, ventilated room.

5. Nomenclature

A_{ij}	surface of the border between two zones i and j
Ar_o	Archimedes' initial jet number
b_o	initial width of jet
Cd	discharge coefficient
Cp	air specific heat
g	acceleration of gravity
h	zone height
m_{ij}	mass flow rate between two zones i and j
me	exhausted air mass flow rate
ms	supplied air mass flow rate
m_o	jet discharge air mass flow rate
P	zone pressure
P_{conv}	convective heat power of emitter
P_{tot}	total heat power of emitter
$Q(z)$	heat flow in thermal plume
T	zone air temperature
Ts	supplied air temperature
u,v,w	velocity components
x,y,z	coordinates
z_o	virtual origin of thermal plume

Greek symbols

Φ_{conv}	convective heat flux exchanged along a wall
ρ	air density

References

[1] Y. Li and S. Holmberg, General flow and thermal condition in indoor airflow simulation, *Build. Environ.*, *29* (1994) 275–281.

[2] J. Lebrun and Ph. Ngendakumana, Air circulation induced by heating emitters and corresponding heat exchanges along the walls: test room results and modelling, *Proc. ROOMVENT '87, Stockolm, Sweden, 1987,* Session 2a, Paper 6.

[3] A.T. Howarth, The prediction of air temperature variations in naturally ventilated rooms with a convective heating, *Build. Serv. Eng. Res. Technol.*, *6* (1985) 169–175.

[4] C. Inard and D. Buty, Simulation of thermal coupling between a radiator and a room with zonal models, *Proc. 12th AIVC Conf., Ottawa, Canada, 1991,* Vol. 2, pp. 125–131.

[5] H. Overby and M. Steen-Thode, Calculation of vertical temperature gradients in heated rooms, *Proc. CLIMA 2000, Oslo, Norway, 1991,* Section B1-5, Paper 25.

[6] H. Bouia, Modélisation simplifiée d'écoulements de convection mixte internes: application aux échanges thermo-aérauliques dans les locaux, *Thèse de Doctorat,* Université de Poitiers, France, 1993.

[7] E. Wurtz and J.M. Nataf, Validation des modèles zonaux décrits par l'environnement orienté objet SPARK, *Proc. European Conf. Energy Performance and Indoor Climate in Buildings, Lyon, France, 1994,* pp. 785–790.

[8] S.V. Patankar, *Numerical Heat Transfer and Fluid Flow*, McGraw Hill, London, UK, 1980.

[9] B.H. Shaw and W. Whyte, Air movement through doorways: the influence of temperature and its control by forced air flow, *Build. Serv. Eng. J. Inst. Heat. Vent. Eng.*, *42* (1974) 210–218.

[10] M.I. Grimitlyn and G.M. Pozin, Fundamentals of optimizing air distribution in ventilated spaces, *ASHRAE Trans., Part 2,* (1993) 1128–1138.

[11] N. Rajaratnam, *Turbulent Jets*, Elsevier Scientific, New York, USA, 1976.

[12] C. Inard, Contribution à l'étude du couplage thermique entre une source de chaleur et un local, *Thèse de Doctorat,* INSA de Lyon, France, 1988.

[13] F. Allard, C. Inard and J.P. Simoneau, Phénomènes convectifs intérieurs dans les cellules d'habitation. Approches expérimentales et numériques, *Rev. Gén. Therm.*, *29* (340) (1990) 216–225.

[14] W.H. Press, S.A. Teukolsky, W.T. Vetterling and B.P. Flannery, *Numerical Recipes in Fortran. The Art of Scientific Computing,* Cambridge University Press, Cambridge, UK, 2nd edn., 1992.

[15] F. Allard, J. Brau, C. Inard and J.M. Pallier, Thermal experiments of full-scale dwellings cells in artificial conditions, *Energy Build.*, *10* (1987) 49–58.

[16] J. Maalej, Emetteurs de chaleur dans les bâtiments et étude des performances, *Thèse de Doctorat,* Université de Valenciennes et du Haut-Cambresis, France, 1994.

[17] Moderate thermal environments. Determination of the PMV and PPD indices and specifications of the conditions for thermal comfort, *ISO 7730,* International Standards Organization, Geneva, Switzerland, 1984.